Attosecond photoelectron spectroscopy of electron tunneling in a dissociating hydrogen molecular ion

Gräfe, Stefanie; Engel, Volker; Ivanov, Misha Yu.

National Research Council Canada   Conseil national de recherches Canada

Canada

Attosecond Photoelectron Spectroscopy of Electron Tunneling
in a Dissociating Hydrogen Molecular Ion

Stefanie Gräfe,[1,2] Volker Engel,[3] and Misha Yu. Ivanov[1]

[1]*Steacie Institute for Molecular Sciences, National Research Council Canada, 100 Sussex Drive, ON Ottawa, K1A 0R6 Canada*
[2]*Institute for Theoretical Physics, Vienna University of Technology, Vienna, Austria*
[3]*Institut für Physikalische Chemie, Universität Würzburg, Am Hubland, 97074 Würzburg, Germany*

We demonstrate the potential of intense-field pump, attosecond probe photoelectron spectroscopy to monitor electron tunneling between the two protons during dissociative ionization of the hydrogen molecule, with attosecond temporal and Angstrom-scale spatial resolution.

The advent of attosecond pulses has opened a route to real-time observation of electronic dynamics. Modern attosecond pulses are phase-locked to the optical oscillations of the intense infrared (IR) pulse used for their generation. The combination of such an IR pulse and the attosecond pulse form the pump-probe pair in attosecond spectroscopy [1,2].

We show how time-resolved photoelectron spectra, recorded with the combination of an intense IR pump and a weak attosecond extreme ultraviolet (XUV) probe, can be used to monitor attosecond dynamics of electron tunneling between the two protons in a dissociating hydrogen molecular ion. Clear information about the electron motion can be extracted from the time-resolved photoelectron spectra by monitoring left-right asymmetries in the photoelectron distribution. These asymmetries track the bound electron motion [3,4].

Our key result is that the information about electron tunneling can be recovered even for a complex correlated electronic-vibrational wave packet in H_2^+, which exhibits no localization in the nuclear or electronic coordinates. The molecular ion is produced from neutral H_2 by a sequence of ionization events at different cycles of the intense IR pump. The resulting wave packet in H_2^+ is spread over a large range of internuclear distances R, and the electron can be tunneling in opposite directions at different R. Nevertheless, despite the large spectral width of the probe pulse, energy-resolved photoelectron spectra monitor the electron motion in the dissociating H_2^+.

Consider a setup similar to the recent experiment [5]; see Fig. 1. An intense few-cycle linearly polarized IR pump pulse interacts with a hydrogen molecule H_2. The pulse induces ionization, producing a pair electron-hydrogen ion H_2^+. The liberated electron, slaved to the optical oscillations of the electric field, recollides with H_2^+ and excites it to the dissociative electronic state $^2\Sigma_u^+$. As H_2^+ dissociates into H and H^+, the second electron bound in H_2^+ tunnels between the two protons before localizing on one of them. The process is controlled by the IR pulse, in particular, its carrier-envelope phase [5–8].

To image the tunneling, we take an attosecond XUV probe, polarized parallel to the IR pump; see Fig. 1. The absorption of one XUV photon catches the electron while tunneling between the two protons, promoting it to the continuum. We calculate the energy-resolved asymmetries in the number of electrons going to the left and right detectors placed along the polarization of both pulses, as a function of the XUV arrival time t_X. This asymmetry tracks the direction of the electron motion [3,4]. Ionization at larger R will result in higher photoelectron energies E, allowing one to obtain both temporal and spatial information.

To model the dynamics of the two electrons and two protons in an intense laser field, we use our approach from Ref. [9]. It divides the process into two steps.
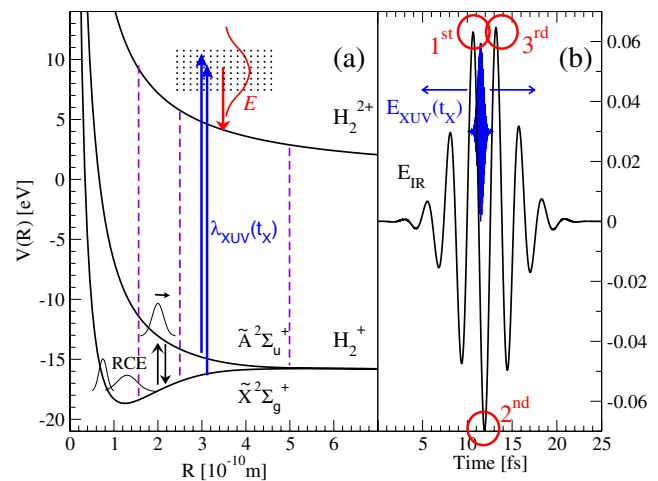
FIG. 1 (color online).   Attosecond probing of electron dynamics in H_2^+. (a) A vibrational wave packet in the ground state $^2\Sigma_g^+$ is created by strong-field ionization of H_2. As it moves towards larger R, the recollision of the liberated electron with the parent H_2^+ excites it into the dissociative state $^2\Sigma_u^+$ (RCE). A time-delayed XUV probe monitors the dynamics in H_2^+ by one-photon ionization (creating H_2^{2+}). (b) The pump-probe pair: an intense few-cycle IR pulse and an attosecond XUV pulse. The IR pulse has a carrier of $\lambda = 800$ nm and is 5 fsec long; the XUV pulse is centered at $\lambda = 15$ nm and is 350 asec long.

The first step includes one-electron ionization of the neutral and the recollision-induced excitation of the ion. It is modeled by solving the fully correlated two-electron time-dependent Schrödinger equation, treating the nuclear motion during the fraction of the laser cycle between the ionization and the recollision classically. The two-electron wave function is then used to extract an "effective recollision field"—the time-dependent electron-electron interaction potential responsible for the excitation of the bound electron in H_2^+. The extracted field is explicitly associated with the excitation from the $^2\Sigma_g^+$ to the $^2\Sigma_u^+$ state of H_2^+ [9]. At the second step, we use the IR field together with the effective recollision field to simulate the dynamics in H_2^+, treating both the electron and the nuclear motion quantum-mechanically.

Ionization of H_2 comes in several bursts centered around the peaks of the oscillating IR field; see Fig. 1(b). The peaks yielding significant ionization are labeled 1–3. Each leads to its own recollision followed by the dissociation of H_2^+. The photoelectron spectra generated by the XUV probe will include the contributions from each of the bursts. Hence, the calculations for the second step are repeated for each burst, with relevant contributions weighted according to the corresponding ionization probabilities. As demonstrated in Ref. [10], the photoelectron spectra from each ionization burst have to be added incoherently, since we are tracing out one of the entangled particles—the first (recolliding) electron.

The calculations are done for the IR pulse $\mathcal{E}_{IR}(t) = \mathcal{E}_0 f(t)\cos(\omega t + \phi)$. The frequency ω corresponds to $\lambda = 800$ nm, the carrier-envelope phase is $\phi = -\pi$, the envelope $f(t)$ is Gaussian with full width at half maximum FWHM = 5 fsec, and the intensity is $I = 1.7 \times 10^{14}$ W/cm^2.

To model each ionization burst for H_2, we confine both electrons and the nuclear coordinate R to one dimension each as in Refs. [9,11], using the soft-core potentials [12]

$$\hat{U}(\xi, R) = -\sum_{\pm} \frac{1}{\sqrt{(\xi \pm R/2)^2 + \varepsilon_{en}(R)}},$$

$$\hat{V}_{ee}(x, y) = \frac{1}{\sqrt{(x - y)^2 + \varepsilon_{ee}(R)}} \quad (1)$$

for the electrons ($\xi = x, y$) and standard Coulomb interaction for the nuclei. The functions $\varepsilon_{en}(R)$ and $\varepsilon_{ee}(R)$ were suggested by Charron [11]. They yield the correct equilibrium distance $R_{eq} = 0.74$ Å for the neutral, good approximation for the H_2 ionization potential $I_p = 17.4$ eV and well approximate the $^2\Sigma_g^+(R)$ and $^2\Sigma_u^+(R)$ surfaces of the ion. We denote these surfaces $V_g(R)$ and $V_u(R)$ and the corresponding Born-Oppenheimer electronic wave functions $\phi_g(x, R)$ and $\phi_u(x, R)$. At R_{eq}, $\varepsilon_{en}(R_{eq}) = 1.0734$ and $\varepsilon_{ee}(R_{eq}) = 0.95833$ a.u.

Now we can simulate the H_2^+ dynamics for each ionization burst. For the ionization burst centered around t_i ($i = 1, \ldots, 3$), we start the calculation in H_2^+ at time $t_i +$

$\pi/(2\omega)$, with the vibrational wave packet centered around the equilibrium distance of H_2. This avoids polarization effects caused by a nonzero IR field but neglects the nuclear motion during the first quarter of the IR oscillation period (0.6 fsec).

We partition our system, confining the H_2^+ to the $^2\Sigma_g^+$ and $^2\Sigma_u^+$ states within the Born-Oppenheimer approximation, and perturbatively treat the XUV-induced transition to the ionic states in H_2^{2+}. The molecular axis is parallel to the polarizations of both IR and XUV fields. The wave function $\Psi(t) = \chi_g(R, t)\phi_g(x, R) + \chi_u(R, t)\phi_u(x, R)$ contains the vibrational wave packets $\chi(R)$ in the gerade [$\phi_g(x, R)$] and ungerade [$\phi_u(x, R)$] electronic states. The Schrödinger equation is

$$i\frac{\partial}{\partial t}\begin{pmatrix} \chi_g(R, t) \\ \chi_u(R, t) \end{pmatrix} = \left[\hat{T} + \begin{pmatrix} V_g(R) & -\mu_{gu}(R)\mathcal{E}(t) \\ -\mu_{ug}(R)\mathcal{E}(t) & V_u(R) \end{pmatrix} \right]$$
$$\times \begin{pmatrix} \chi_g(R, t) \\ \chi_u(R, t) \end{pmatrix}. \quad (2)$$

Here $\hat{T}$ is the kinetic energy operator, and $\mu_{gu}(R)$ is the transition dipole between the gerade and the ungerade state. The driving field $\mathcal{E}(t)$ includes the intense IR field $\mathcal{E}_{IR}(t)$ and the effective recollision field.

At a variable time delay t_X, an attosecond XUV probe centered around t_X ionizes H_2^+; see Fig. 1. We assume a Gaussian envelope with FWHM = 350 asec and a carrier wavelength $\lambda_{XUV} = 15$ nm. Ionization of H_2^+ by the XUV pulse is modeled using first-order perturbation theory in the XUV field, thereby distinguishing between the contributions with positive and negative momentum, respectively. The ionic potential and the intense IR field are included nonperturbatively, using the strong-field eikonal-Volkov approach (SF-EVA) developed in Refs. [4,13–15], shown to be quantitatively accurate for both intense-field ionization and laser-assisted XUV ionization. Technically, we follow the recipe developed in Ref. [14], writing the amplitude to find the electron with the final momentum p as

$$c_p(t_X, R) = -i\int_0^T dt \int dk \langle p|\hat{U}(T, t)|k\rangle\langle k|\hat{V}_X(t - t_X)|\Psi(t)\rangle. \quad (3)$$

Here $T \to \infty$, $\hat{V}_X(t - t_X) = x\mathcal{E}_{XUV}(t - t_X)$ is the interaction with the XUV probe pulse, $\hat{U}(T, t)$ is the eikonal-Volkov propagator [14], and $|k\rangle$ and $|p\rangle$ are the *field-free* continuum states with the asymptotic momenta k and p, respectively, in the eikonal approximation: $\langle x|k\rangle \approx \exp[i\Phi(k, x, R)]/\sqrt{2\pi}$, where

$$\Phi(k, x, R) = ikx - \frac{1}{k}\int_0^x U(x', R)dx' \quad (4)$$

and $U(x, R)$ is given by Eq. (1).

The coupling between the ionic potential and the intense IR field is hidden in the matrix element $\langle p|\hat{U}(T, t)|k\rangle$. In the absence of the laser field, $\langle p|\hat{U}(T, t)|k\rangle = \delta(p - k)$. In the

strong-field approximation (SFA), which neglects the ionic potential, it is

$$\langle p|\hat{U}^{(\text{SFA})}(T, t)|k\rangle = \delta(p + A_L(t) - k)e^{-(i/2)\int_t^T [p+A_L(\tau)]^2 d\tau}.$$
(5)

Here $A_L(t)$ is the vector potential of the IR field. When the ionic potential is included, the delta function is broadened and its maximum is shifted, as analyzed in Ref. [14]. In our conditions of large XUV-photon energy, the changes are small compared to the characteristic momentum $k \sim 2$ and the bandwidth of our XUV pulse. This allows us to further simplify the SF-EVA approach by setting $\langle p|\hat{U}(T, t)|k\rangle = \langle p|\hat{U}^{(\text{SFA})}(T, t)|k\rangle$ in Eq. (3). The effect of the ionic potential on the liberated electron enters via the XUV transition matrix elements in Eq. (3), which include the ionic potential [see Eq. (4)]. The nuclear part of the continuum wave packet is propagated using the split-operator technique, with the nuclear propagator $U_{\text{nuc}}(T, t) = \exp(-idt/2\hat{T}) \times \exp[-idt V_{\text{H}_2^+}(R)] \exp(-idt/2\hat{T})$ on a grid with 256 points, with a step size of $dR = 0.05$ a.u.

The photoelectron spectra are calculated as

$$S(p, t_X) = \int dR |c_p(t_x, R)|^2.$$
(6)

The calculated photoelectron spectrum (weighted with the probability ionizing H_2 to H_2^+) for the left detector is shown in Fig. 2. As the nuclei move towards larger R, the ionization potential of H_2^+ decreases, yielding higher photoelectron energy (*reflection principle*) [16]. No signatures of tunneling are immediately apparent. We note that, for the short pump pulse, most times the XUV probes nearly field-free dynamics.

Although before the most probable ionization event (around 12 fsec) no H_2^+ is produced, the XUV pulse might ionize neutral H_2 leading to an additional photoelectron signal. However, since electron tunneling between the two dissociating protons occurs only in H_2^+, the XUV signal from H_2 will contain no associated left-right asymmetry
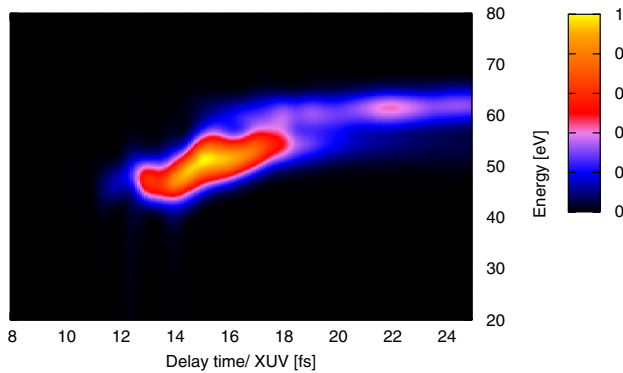

FIG. 2 (color online). Photoelectron spectra on the left detector as a function of the XUV probe delay time t_X. XUV duration is 350 asec; the wavelength $\lambda_{\text{XUV}} = 15$ nm. The vertical scale, shown as a color bar, is in arbitrary units.

discussed below. Apart from streaking, it provides constant background, subtracted in our calculation.

To track electron tunneling, we need to look at the difference between the number of electrons arriving to the left and the right detectors. Quantum-mechanically, due to the symmetry of the gerade and ungerade states, the corresponding matrix elements $\mu_g(k, R) = \langle k|x|\phi_g\rangle$ and $\mu_u(k, R) = \langle k|x|\phi_u\rangle$ are exactly $\pi/2$ out of phase, the former being purely imaginary and the latter being real. Hence, the maximal constructive (or destructive) interference during the one-photon transition to the continuum state $|k\rangle$ from the states $|g\rangle$ and $|u\rangle$ requires that the wave packets χ_u and χ_g in $|\Psi(t)\rangle = \chi_g(R, t)|g\rangle + \chi_u(R, t)|u\rangle$ are also $\pm\pi/2$ out of phase. The $\pm\pi/2$ phase shift between χ_g and χ_u corresponds to the electron being exactly in the middle of tunneling between the two nuclei. At the same time, the maximal localization of the electron on one of the nuclei corresponds to χ_g and χ_u in phase or π out of phase. This phase relationship eliminates the interference between the gerade and the ungerade states and yields zero asymmetry.

Dealing with the asymmetry, one faces several issues. First, the relative phase between $\chi_g(R, t)$ and $\chi_u(R, t)$ depends on R. At different R in the vibrational wave packet in H_2^+, the electron could be tunneling in opposite directions. To deal with this issue, it is preferable to use energy-resolved asymmetries, since the energy of the photoelectron created by ionizing H_2^+ is quite sensitive to R for the range of interest $R \sim 2$–4 Å. This limits the bandwidth of the XUV probe, preventing one from using XUV probe pulses which are too short.

Second, H_2^+ dissociation is induced by several H_2 ionization or recollision events. In principle, the two successive recollision events a half-cycle apart are mirror images of each other. Therefore, it is natural to expect that they will result in the electron tunneling in H_2^+ in opposite directions. This is indeed the case—but only for the *same delay after recollision*. Fortunately, these two events are also delayed by a half-cycle, so that for a given probing time t_X the time delay after the recollision for the two events is different. In fact, at the initial stage of dissociation the electron tunneling is slaved to the strong driving field and proceeds in the same direction for both events, for fixed t_X.

Third, the asymmetry is introduced not only by the electron motion inside the molecule before ionization but also by the IR field-induced streaking after ionization. For high XUV-photon energies, the final p and the initial k electron momenta are related by $p = k - A_L(t_X)$. For the initial momenta in opposite directions k and $-k$, the final energies are different. To monitor the asymmetry due to electron tunneling, we remove this streaking by recalibrating the final momenta p at the detector to the initial momenta k after ionization using the relationship $k = p + A_L(t_X)$.

The asymmetry calculated for the first ionization event is displayed in Fig. 3(a). The asymmetry is defined as
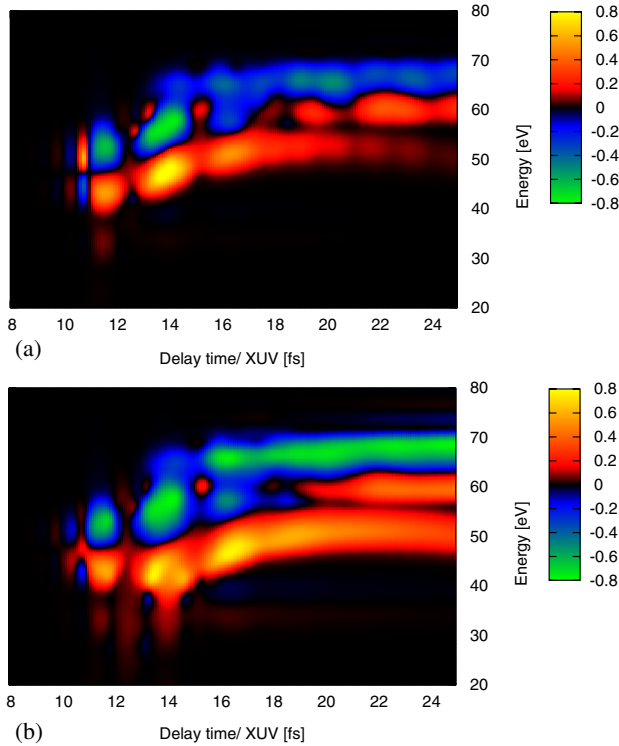
FIG. 3 (color online).   (a) shows the contribution of the first H_2 ionization event to the asymmetry in the photoelectron spectra between the left and the right detector. (b) shows the total asymmetry in the photoelectron spectra between the left and the right detector, including all ionization events weighted by their respective probabilities. Positive asymmetry corresponds to higher signal at the left detector. The XUV probe pulse is 350 asec; the wavelength $\lambda_{XUV} = 15$ nm.

$(S_{left} - S_{right})/(S_{left} + S_{right} + S_0)$, where S_0 is 0.01 of the maximum value of $S_{left} + S_{right}$. The color-coded scale in Fig. 3 is dimensionless. Several things are apparent. First, the asymmetry oscillates for a given final energy, say, $E = 60$ eV ($R \approx 2.5$ Å). This reflects the change in the direction of the electron tunneling at a given R. Second, immediately after ionization the asymmetry goes from maximum to zero in about a half-period of the driving IR field, reflecting the fact that the electron motion is slaved to the laser field. Third, at long delay times, as the vibrational wave packet moves to large R, the oscillations slow down until tunneling freezes and the asymmetry tends to zero.

Figure 3(b) shows the total asymmetry, with the contributions of all ionization events included. Note that the left-right asymmetries can reach almost 100%. Qualitatively, the results are similar to those in Fig. 3(a), even though the overlap of several ionization events masks fine details of the electron tunneling. For a final electron energy between 55 and 65 eV, i.e., for R between 1.5 and 5 Å, the overall direction of electron tunneling changes with time. For electron energies above $E \sim 65$ eV, corresponding to $R \gtrsim 5$ Å, the direction of tunneling freezes. Unlike in Fig. 3(a),

where the asymmetry decays at large t_X, here the asymmetry remains for longer times due to the much more extended vibrational wave packet, which is generated by dissociative ionization during the whole IR pulse and includes very slow components.

In conclusion, we have demonstrated the possibility of using pump-probe ionization spectroscopy to resolving electron tunneling on the attosecond time scale. Ionization of the neutral hydrogen molecule and subsequent excitation and dissociation of the molecular ion are induced by an intense few-cycle infrared pulse, which acts as a pump. A time-delayed attosecond XUV pulse ionizes H_2^+, probing the coupled nuclear-electronic dynamics. The electron momentum prior to ionization leads to pronounced asymmetries in the direction of its propagation after ionization, allowing one to extract information about electronic motion by monitoring asymmetries in the photoelectron distribution. Additionally, the photoelectron kinetic energy distribution as a function of the delay time directly reflects the nuclear motion. Therefore, temporal resolution of the electron tunneling dynamics is accompanied by spatial information on the nuclear dynamics.

[1] M. Drescher *et al.*, Nature (London) **419**, 803 (2002).
[2] M. Uiberacker *et al.*, Nature (London) **446**, 627 (2007).
[3] G. L. Yudin, A. D. Bandrauk, and P. B. Corkum, Phys. Rev. Lett. **96**, 063002 (2006).
[4] O. Smirnova, M. Spanner, and M. Ivanov, J. Phys. B **39**, S323 (2006).
[5] M. Kling *et al.*, Science **312**, 246 (2006).
[6] P. Haljan *et al.*, Laser Phys. **7**, 839 (1997).
[7] X. M. Tong and C. D. Lin, Phys. Rev. Lett., **98**, 123002 (2007).
[8] F. He, C. Ruiz, and A. Becker, Phys. Rev. Lett. **99**, 083002 (2007).
[9] S. Gräfe and M. Yu. Ivanov, Phys. Rev. Lett. **99**, 163603 (2007).
[10] H. Niikura *et al.*, Nature (London) **417**, 917 (2002); **421**, 826 (2003).
[11] E. Charron, A. Giusti-Suzor, and F. H. Mies, Phys. Rev. Lett. **71**, 692 (1993); E. Charron (private communication).
[12] J. Javanainen, J. H. Eberly, and Q. Su, Phys. Rev. A **38**, 3430 (1988).
[13] O. Smirnova, M. Spanner, and M. Ivanov, J. Phys. B **39**, S307 (2006).
[14] O. Smirnova *et al.*, J. Phys. B **40**, F197 (2007).
[15] O. Smirnova, M. Spanner, and M. Ivanov, Phys. Rev. A **77**, 033407 (2008).
[16] M. Braun, C. Meier, and V. Engel, J. Chem. Phys. **105**, 530 (1996).